Hindawi
Geofluids
Volume 2022, Article ID 3383773, 12 pages
https://doi.org/10.1155/2022/3383773

Research Article

Fractal Characteristics of the Seepage Erosion Process in Porous Soil

Yu Wang,[1] **Xiangbao Duan**,[2] **Yanchang Gu**,[2] **and Shijun Wang**[2]

[1]*College of Architectural Engineering, Jiangsu Open University, No. 399, The North Road of Jiangdong, Nanjing, Jiangsu, China*
[2]*Nanjing Hydraulic Research Institute, No. 223, Guangzhou Road, Nanjing, Jiangsu, China*

Correspondence should be addressed to Yu Wang; wangyu@jsou.edu.cn

Received 5 January 2022; Revised 24 April 2022; Accepted 6 May 2022; Published 26 June 2022

Academic Editor: Wensong Wang

Seepage-induced erosion in porous soil has always been a major concern in the field of geofluids. Various fractal models have been built to theoretically investigate the porosity and permeability coefficient. However, the seepage erosion process (i.e., incubation, formation, evolution, and destruction) in porous soil is not clearly demonstrated to clarify the seepage fractal characteristics. In this paper, a series of hydraulic tests were performed to reveal the mass fractal characteristics of sandy gravels, coarse-grained sands, and fine-grained sands in the seepage erosion process. The results show that the mass fractal dimension was appropriate to describe the cumulative mass distribution of particles, the complexity of pore networks, and the dynamic changes of the seepage erosion process. Moreover, the scale-invariant interval, as an essential precondition for the accurate calculation of the mass fractal dimension, was to some extent affected by the average grain size and the fine content of porous soil. In particular, the changing trend of porosity and permeability coefficient with the mass fractal dimension was demonstrated in the seepage erosion process. Both porosity and permeability coefficients indicated an increasing trend as the development of seepage erosion. However, the mass fractal dimension gradually decreased due to the removal of fine particles induced by seepage flow water. Research findings will not only provide a new perspective on the seepage erosion mechanism but also predict the development of the seepage erosion process in engineering practice.

1. Introduction

Porous soil is one of the most commonly used filling materials in hydraulic engineering and geotechnical foundation works. The physical structure of porous soil presents irregular, discontinuous, and nonhomogeneous characteristics, which derive from the randomness of particle size distributions and pore networks [1–3]. For this reason, porous soil is more likely to trigger seepage erosion due to the loss of soil integrity caused by seepage flows, which may bring the risk of potential disaster, such as sinkholes in roads, the collapse of foundation pits, and the breaching of dams [4–7]. Given the transport of fine particles from pore networks, the problem of seepage erosion in porous soil can be more complex. There is a need for theories and models to investigate the essential characteristics of seepage erosion in porous soil, thereby ensuring the long-term safety of project operation.

Despite the complication of solid particles and pore networks, previous studies have confirmed that porous soil statistically presents fractal characteristics [8–11]. Fractal, first introduced in detail by Mandelbrot and widely used in various aspects of natural science, offers a unique opportunity towards a rational basis for the complexity of soil properties [12]. An essential feature of the fractal theory is self-similarity observed in natural objects or processes with no exception for porous soils. A self-similar soil, that is, a part of the whole, constantly resembles the whole, sometimes only in a statistical sense [13–15]. Therefore, porous soil can be divided into some similar entities along with further subdivisions into similar entities. The fractal dimension can be regarded as the quantity index to describe the self-similar degree or complexity of porous soils [16–19]. Originally, the fractal dimension of porous soil was found to account for fragmentation processes including explosive disruption, impact shattering, weathering, and crushing.

Differed in soil fragmentation, the seepage erosion process also presents fractal characteristics, because fine particles transport by seepage flow from pore networks [20]. Concretely, finer fractions may migrate along with seepage flow at a certain hydraulic gradient, and then, the pore size and the permeability coefficient are changed, which in turn drives the further transport of coarser fractions. The cycle constantly repeats, resulting in seepage erosion with the increasing hydraulic gradient.

Whether seepage erosion occurs or not largely depends on the soil properties and hydraulic conditions. The hydraulic conditions can be controlled in the laboratory tests or field tests, while the soil properties, especially the permeability and porosity, play a more important role in the seepage erosion process. Numerous models have been developed to predict the permeability of porous soil [21–25]. For example, assuming that the porous network is simplified down to a bundle of capillary channels, the Hagen-Poiseuille equation is proposed to calculate the seepage flow velocity in a capillary tube [4, 13]. For a better description of the complicated seepage flow in porous soils, Kozney and Carman [4, 14] derived a famous expression for the permeability coefficient K given by

$$K = \left(\frac{\gamma}{\mu}\right)\left(\frac{1}{k_0 T^2 {s_0}^2}\right)\left(\frac{e^3}{1+e}\right), \tag{1}$$

where γ is the unit weight of fluid, μ is the dynamic viscosity of fluid, k_0 is the pore shape factor, T is the pore tortuosity, s_0 is the specific surface area of soils, and e is the void ratio. However, it has been proven that the measured value and the calculated value of the permeability coefficient do not always agree. Some studies have shown that the difference is mainly caused by the presence of unequal pores and the empirical KC constant. To better clarify the physical meaning of the KC constant, Yu and Cheng [26] were the first to establish a fractal model for the permeability coefficient of porous media as follows:

$$K = \frac{\pi}{128}\frac{L^{1-D_T}}{A}\frac{D_\mathrm{f}}{3+D_T-D_\mathrm{f}}\lambda_{\max}^{3+D_T}, \tag{2}$$

which demonstrates that the permeability is a function of the tortuosity fractal dimension D_T, the pore fractal dimension D_f, and structural parameters, A, L, and $\lambda_{\max}$. If a straight capillary model ($D_\mathrm{T} = 1$) is assumed, equation (2) can be reduced to

$$K = \frac{\pi}{128}\frac{1}{A}\frac{D_\mathrm{f}}{4_T-D_\mathrm{f}}\lambda_{\max}^4, \tag{3}$$

which indicates that the permeability coefficient is very sensitive to the maximum pore size $\lambda_{\max}$, and the greater the pore fractal dimension D_f, the larger the permeability coefficient K. Yu and Cheng's model greatly improves the understanding of the permeability coefficient, since every parameter in the equation is clear and significant, which is verified by many experimental results of different porous media. As long as the parameters are determined, the permeability coefficient can be precisely predicted. The pore fractal dimension D_f is generally obtained by the box-counting method or the approximation of self-similarity based on the Sierpiński-type gasket model [27, 28]. The tortuosity fractal dimension D_T can also be determined by the box-counting method [29]. The maximum pore size $\lambda_{\max}$ is usually acquired from the scanning electron microscope (SEM) observation and mercury injection data analysis [3, 24]. Since these parameters are difficult to obtain, a mass fractal model was developed assuming pore size to follow a simple relationship as a function of particle size [30–32]. The hypothesis that the smaller the pore size, the larger the tortuosity was extended to express as a function of pore diameter. This relationship has been incorporated into the capillary flow model to obtain the permeability coefficient of unsaturated soils. Interestingly, it has been accepted for many years that the permeability coefficient of porous soil is largely governed by both pore and particle properties with fractal characteristics including size, area, volume, and mass. The pore-solid fractal approach was employed to simulate soil structure by simultaneously considering the solid fraction and pores [33–36]. The particle size distribution curves of testing soils were used to explore the fractal relationship between the permeability coefficient and the porosity. The porosity of soil with arbitrary particle size distribution and particle shape was controlled by a group of "smallest particles" related to the permeability coefficient [37–40].

The foregoing studies have demonstrated the fractal characteristics of pore networks and solid particles, but seepage in porous soil, which flows through pore networks, should be fractal with some other special characteristics [41, 42]. Furthermore, the seepage erosion process could also present fractal characteristics because fine particles transport from pore channels rather than soil fragmentation. For example, the suffusion is one of seepage erosion forms to describe the phenomenon of geotechnical foundations, in which the finer fraction of the soil moves through the voids of the coarser fraction without any loss of matrix integrity or change in total volume. Another common seepage erosion in hydraulic engineering is backward piping erosion, which shows that the soil particles are detached from the downstream exit of seepage flow and gradually develop along the direction of flow direction [15, 43]. Whatever form seepage erosion takes, soil particles are constantly washed out with an increasing hydraulic gradient, resulting in the increase in the porosity and the permeability coefficient, which dramatically changes the hydromechanical characteristics of the soil, thus inevitably bringing potential engineering hazards. For instance, the February 2017 failure of the spillway chute at Oroville Dam, owned and operated by the California Department of Water Resources (DWR), raises great concerns for joints and fractures of concrete spillway chutes that could allow penetration of high-pressure water into a chute foundation. Investigations have shown that seepage-induced erosion of porous soil in the foundation is the most likely reason for the initial chute slab failure under high-pressure flow conditions [44, 45].

Previous studies have gained a better understanding of the permeability coefficient in porous media based on various fractal models in theory. However, the seepage erosion process in porous soil is not clearly or fully tested to clarify the seepage fractal characteristics. This paper, which is restricted to sandy gravel, coarse-grained sand, and fine-grained sand, has three purposes. First, a mass fractal model will be used to analyze the scale-invariant intervals of different soil samples, thereby clearly determining the physical meaning of the mass fractal dimension in porous soil. Second, a series of hydraulic tests will be conducted to show the seepage behavior of the entire erosion process (i.e., incubation, formation, evolution, and destruction) through the observations of the hydraulic gradient, overflow amount, and sand boiling amount. Third, the mass fractal dimension will be used to evaluate the fractal characteristics of the seepage erosion process in porous soil. Research findings will help better understand the mechanism of the seepage erosion process and reduce the risk of seepage failure in practical engineering.

2. Materials and Methods

2.1. Testing Soils. Tests were performed on granular soils from the banks of the Yangtze River, including four samples of sandy gravels numbered 1~4 (Figure 1), two samples of coarse-grained sands numbered 5~6 (Figure 2), and two samples of fine-grained sands numbered 7~8 (Figure 2). Soils were prepared to compare various hydraulic parameters of the initial seepage erosion process. In particular for seepage erosion tests, the hydraulic pressures, overflow amounts, and sand boiling amounts were measured to show the critical hydraulic gradient leading to seepage erosion. Also, soil samples were taken as follows. The cutting edge was used to press vertically into natural soils until they were filled in the ring sampler; then, surrounding soils were cut off and the ring sampler was carefully taken out to keep natural soils undisturbed. For the large-size gravels (maximum grain diameter of 3 cm), an equivalent density method was employed to keep the soil unit weight invariant by using fine particles instead of large ones. The physical property parameters of soils are presented in Table 1.

2.2. Testing Apparatus. A testing apparatus was designed for porous soil to measure hydraulic pressures and gradients under the conditions of vertical seepage flow through a soil sample. A schematic illustration of the apparatus is presented in Figure 3. The general concept of the apparatus is to provide a uniform hydraulic gradient through a soil sample without converging or diverging flow conditions, thereby observing the hydraulic pressures and gradients with measuring equipment. Besides, the necessary conditions for the critical hydraulic gradient to initiate the seepage erosion process can be evaluated. A detailed description of the testing apparatus is exhibited as follows.

The apparatus consists of a water supply device, a sample holder, measuring equipment, and a data collection system. The soil sample is retained in a rigid-walled Plexiglas holder sealed in a porous permeable board, which is attached to a

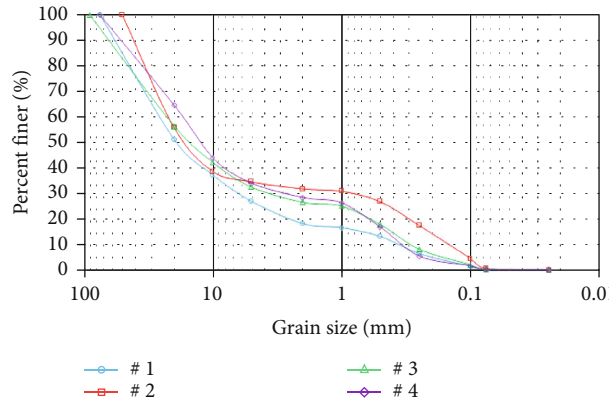

Figure 1: Grading curve of sandy gravels numbered 1~4.

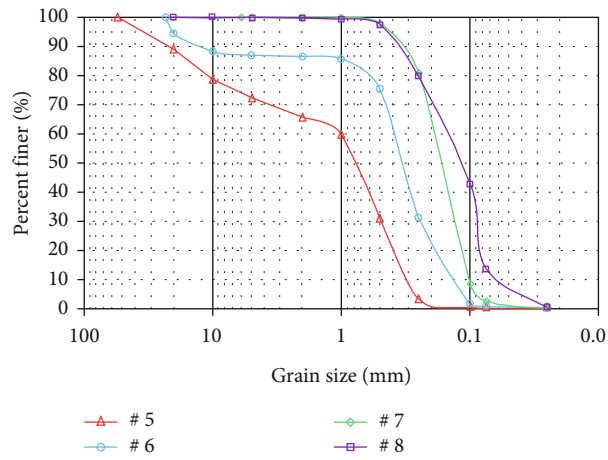

Figure 2: Grading curve of sands numbered 5~8.

conical, stainless, and influent water supply device. The porous permeable board at the base of the cylinder holds up the soil while allowing water to flow gradually into the soil sample. The soil sample holder is a 75.0 cm height and 25.5 cm diameter cylinder-shaped Plexiglas mold with two rows of pore pressure measurement ports located at the holder sides, which is designed to precisely measure the hydraulic pressure of seepage flow through the sample at different locations (Figure 4). Piezometric tubes are used to manually measure pore pressure, and sensors that are connected to the data collection system can automatically measure the hydraulic pressure in real time. To better improve the reliability of monitoring data, measurements are made using 9 pressure sensors (numbered a~i) installed vertically along the side of the apparatus every 5 cm, and 9 piezometric tubes (numbered 0~8) are alternately located on the opposite side every 5 cm, except for no. 0 tube, which is set in the porous permeable board to measure the upstream water head. The resulting spacing along the vertical allowed to acquire measurements every 2.5 cm to observe minor deformation in each part of the soil in the seepage erosion process. The inside of the sample holder is coated with silicone gel that serves a dual function. First, it provides a frictional interface between the soil samples and the sample

Table 1: Physical property parameters of experimental soils.

Soil number	Soil type	Uniformity coefficient C_u	d_{50} (mm)	Porosity N	Dry density ρ_d (g/cm^3)	Permeability coefficient K (cm/s)
1	Sandy gravel	81.25	20.00	0.26	1.96	$3.35E-02$
2	Sandy gravel	73.30	17.00	0.22	2.08	$1.10E-02$
3	Sandy gravel	66.70	15.00	0.24	2.02	$1.02E-02$
4	Sandy gravel	45.70	12.00	0.27	1.94	$1.10E-02$
5	Coarse-grained sand	3.45	0.77	0.32	1.80	$4.00E-02$
6	Coarse-grained sand	3.33	0.32	0.38	1.65	$2.50E-02$
7	Fine-grained sand	1.80	0.15	0.46	1.43	$3.20E-03$
8	Fine-grained sand	2.10	0.11	0.47	1.40	$7.00E-04$

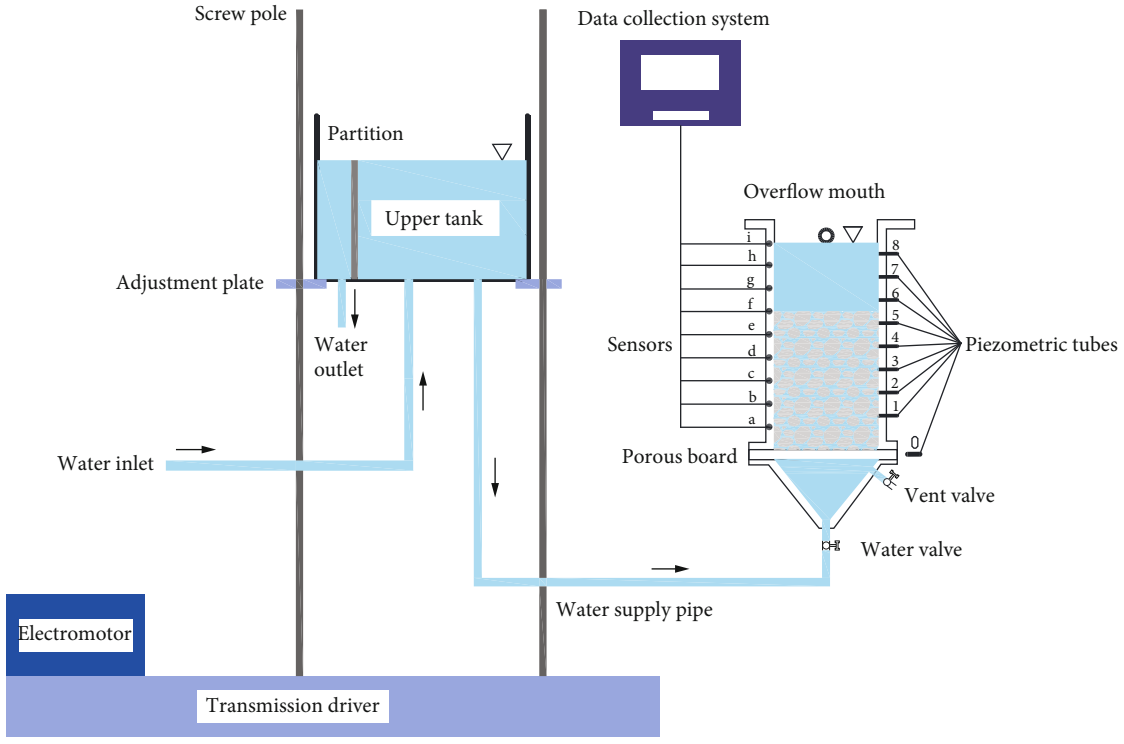

Figure 3: Schematic illustration of testing apparatus.

holder. Second, since porous soil sample indents into the silicon, it prevents a preferred seepage path along the edges of the sample that would occur as a consequence of larger interstitial voids caused by a lack of interlocking with the smooth Plexiglas surface. In addition, a control sample is used to demonstrate that the sensors may not be affected by the transport of particles, silicone gel obstructions, or the potential segregation.

The hydraulic pressure is flexibly governed by the water tank attached to the screw pole to produce a uniform vertical hydraulic gradient upward through a porous permeable board into the sample. The altitude adjustment is controlled by two nuts arranged on the screw pole that can be fixed on the transmission driver, and the hydraulic pressure can be slowly regulated. By controlling the upstream head of the water tank and the downstream head of the overflow mouth, the differential head across the sample is steadily increased until initial seepage erosion occurs. Both seepage behavior and soil deformation of each part of the porous soil can be observed and recorded.

2.3. Testing Procedure. The testing procedure is outlined as follows:

(1) For better control of various factors that could affect the seepage erosion, such as temperature, water content, and physical dimension of soil, the laboratory test was kept at a uniform temperature, and all soil

Figure 4: Physical model of the soil sample holder.

samples were dried and prepared in a completely saturated condition, and the physical dimensions of the soil were rigidly performed

(2) Soils were tested with three specimen heights in the sample holder. If the content of coarse sands was high, the filling height would be high. Specifically, for sandy gravels, the filling height was 35 cm. The filling height was 30 cm for coarse-grained sands, while the filling height was 25 cm for fine-grained sands

(3) Two ways of water injection were used to make the sample soil gradually saturated. One was to inject water continuously to ensure that the initial hydraulic gradient was less than 0.1 and then increase to a slight hydraulic gradient increment of 0.1, which could be observed every five minutes until the hydraulic pressure on the sensors was steady or water level in piezometric tubes varied little. The other was to inject water regularly to simulate the process of water level gradually rising, which was loaded with a tiny hydraulic gradient increment of 0.05~0.1 every 15~30 minutes

(4) The tests went on until the soil completely failed. The test was not stopped until the connected leakage pathway was formed from the bottom to the top of the soil samples, or the soil particles were uplifted to float in entirety. The hydraulic gradient, permeability coefficient, and overflow amount were used as quantificational indexes. Tests ended until these parameters increased more than 10 times

(5) Given the observations of the water head in the piezometric cubes, hydraulic pressure on the sensors, and opacification degree of overflow water, internal adjustments of fine particles were captured during the seepage erosion process. At the same time, the hydraulic gradient and overflow amount were frequently measured to obtain adequate seepage erosion data

3. Results and Discussion

3.1. Mass Fractal Dimension Calculation. Since the fractal dimension is the key factor affecting the permeability coefficient, the calculation of the fractal dimension appears to be particularly important. Given the scale invariance in self-similar characteristics of porous structures, fractal analysis is an appropriate and efficient mathematical tool for assessing porous soil. Most studies of the fractal properties of porous soil are based on the geometric fractal dimension, which is commonly obtained by the box-counting method or image analysis. However, the statistical fractal dimension is more suitable for describing the fractal characteristics in porous soil, because the scale invariance only exists in a certain range of grain size. The mass fractal dimension, as one of the statistical fractal dimensions, is commonly used in practical engineering for the accumulation of particle mass. Moreover, the mass fractal dimension is conveniently acquired based on the grading curve, which is relevant for the particle size distribution of porous soil. Following this concept within the study herein, the mass fractal dimension is used for the quantitative description of the mass accumulation associated with the particle size distribution and the complication of pore networks.

In geotechnical engineering, the grading curve is typically presented as the percentage of the cumulative mass of soil occupied by a given size fraction. The fractal relationship of the mass distribution can be expressed by

$$M(<r) \propto r^{3-D_m}, \tag{4}$$

where $M(<r)$ is the mass of particles whose sizes are smaller than a given comparative size r and D_m is the mass fractal dimension. A relationship based on the results of a standard sieve analysis test was established by Tyler and Wheatcraft (1992) to calculate the fractal dimension of soils. This relationship is

$$\frac{M(R<r)}{M_T} = \left(\frac{r}{r_L}\right)^{3-D_m}, \tag{5}$$

where $M(R<r)$ is the cumulative mass of particles with size R smaller than a given comparative size r, M_T is the total mass of particles, r is the sieve size opening, and r_L is the maximum particle size as defined by the largest sieve size opening used in the sieve analysis. Logarithmic

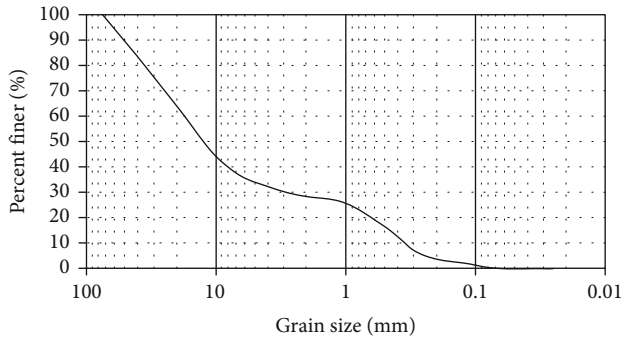

Figure 5: Grading curve of a sample in a sandy gravel.

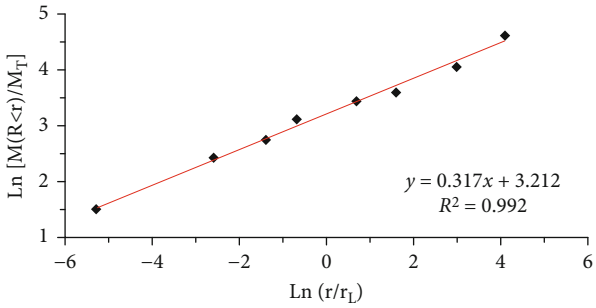

Figure 6: Logarithmic linear fitting curve of a sandy gravel.

transformations of equation (5) on both sides yield the following:

$$L_n \frac{M(R<r)}{M_T} = (3 - D_m) L_n \left(\frac{r}{r_L}\right) + C, \tag{6}$$

where C is the constant. The fractal dimension D_m and the slope K_s of the linear fitting equation of the grading curve in $L_n\, M(R<r)/M_T \sim L_n(r/r_L)$ coordinates satisfy

$$D_m = 3 - K_s. \tag{7}$$

For example, the grading curve of a sandy gravel is shown in Figure 5, and the logarithmic linear fitting curve is illustrated in Figure 6. The slope $K_s = 0.317$; hence, the fractal dimension $D_m = 3 - 0.317 = 2.683$. Beyond that, the correlation coefficient $R^2 = 0.99$ shows that the linear fitting relationship of the grading curve has a high correlativity. Note that the mass fractal dimension represents the cumulative mass feature of soil particles, reflecting the primary physical property of porous soil. Unlike self-similarity or self-affinity of mathematical fractal dimension on the infinite scale, self-similarity of an approximate or statistical fractal object, including porous soil, exists only in a finite scale range. Therefore, the mass fractal dimension calculated by equation (7) is only applicable to a certain scope of soil particles, namely, scale-invariant interval for the statistical self-similarity range of porous soil particles.

The determination of the scale-invariant interval is an essential precondition for the accurate calculation of the mass fractal dimension. The main methods for determining the scale-invariant interval include artificial judgment, correlation coefficient test, and fitting error estimation. Among them, the artificial judgment method is more convenient and more effective, thus avoiding the "drifting" phenomenon of the scale-invariant interval. Herein, adopt the artificial judgment method to determine the scale-invariant intervals of different porous soils. According to the $L_n\, M(R<r)/M_T \sim L_n(r/r_L)$ correlation curve, two inflection points in the middle of which a scatter of points can approximately fit into a straight line. The scale of the straight line is the scale-invariant interval of porous soil. Moreover, the better the correlation of the fitting linear, the more accurate the scale-invariant interval. Results from statistical analysis show the scale-invariant intervals of different soil samples (Figure 7). A series of black arrows represent the inflection points on fitting curves of soil samples, including coarse-grained sands, fine-grained sands, and sandy gravels. The extent of two inflection points corresponding to horizontal ordinate values indicates the range of self-similarity of porous soils. It has been found that there are significant differences among the scale-invariant intervals from different soil samples. Obviously, the larger the average grain size d_{50}, the broader the scale-invariant interval. The scale-invariant interval of sandy gravel ranges from 0.25 mm to 20 mm, while coarse-grained sand ranges from 0.25 mm to 10 mm and fine-grained sand ranges from 0.25 mm to 5 mm. This can be explained by the fact that the fine content of the scale-invariant interval could affect the particle size distribution of porous soil.

3.2. Mass Fractal Dimension Analysis. The slope K_s of the fitting straight line of the scale-invariant interval can be used to figure out the mass fractal dimension D_m. For example, the sample of sandy gravel numbered 1 was used to calculate the mass fractal dimension. The logarithmic linear fitting curve is illustrated in Figure 8. Although fractal analysis can describe irregular, discontinuous, and nonhomogeneous characteristics, it is insufficient to describe the complexity of porous soils by a single fractal dimension. Without considering segmentation data, the mass fractal dimension is $D_m = 3 - 0.92 = 2.08$ and the correlation coefficient is $R^2 = 0.69$ with relatively poor reliability. Through statistical analysis of two separate linear fitting curves, a fractional quantitative characterization of porous soil is presented with high correlativity and good reliability. One linear fitting curve indicates the mass fractal dimension $D_{m1} = 3 - 2.80 = 0.20$ when considering the grain size smaller than 0.25 mm, which means that the degree of soil uniformity is high without fractal characteristics. While the other shows that the mass fractal dimension is $D_{m2} = 3 - 0.16 = 2.84$ and the correlation coefficient is $R^2 = 0.94$ when considering the grain size larger than 0.25 mm. Comparatively, the mass fractal dimension D_{m2} is relevant, since the content of particles with a grain size larger than 0.25 mm is approximately 92%, which primarily affects the physical property of porous soil.

By analogy, the mass fractal dimensions and scale-invariant intervals of different experimental soils are shown in Table 2. The results show that the mass fractal dimension represents the uniformity degree of the soil particle size

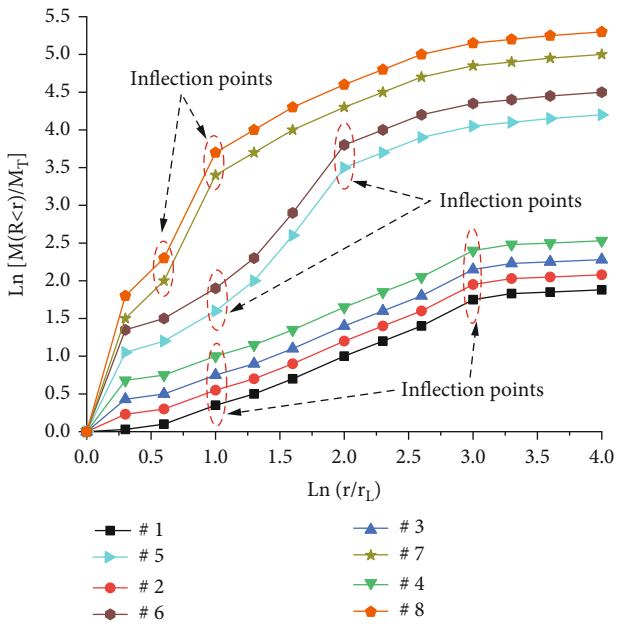

Figure 7: The fitting curves of experimental samples numbered 1~8.

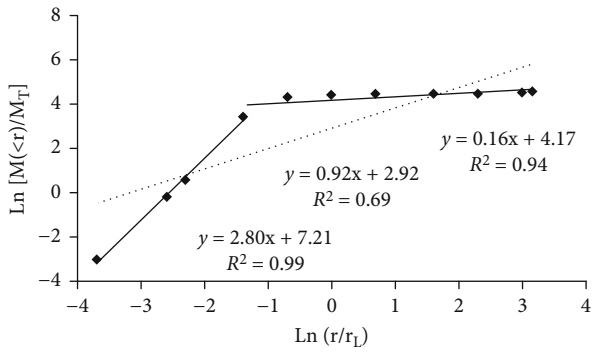

Figure 8: Logarithmic linear fitting curve numbered 1.

distribution associated with pore networks. Moreover, the multifractal dimension of porous soil is closely related to the fine content of the scale-invariant interval. It is evident that both the average grain size and the fine content of the scale-invariant interval are the primary factors influencing the mass fractal dimension. Specifically, for various sandy gravels, the scale-invariant intervals are almost the same, while the higher the fine content of the scale-invariant interval, the larger the mass fractal dimension. Comparing coarse-grained sands with fine-grained sands, an inference can be drawn that the smaller the average grain size, the narrower the scale-invariant interval. Despite the small average grain size and the narrow scale-invariant interval, the mass fractal dimension presents an increasing trend that may be related to the fine content and the uniform coefficient. Anyway, the mass fractal dimension is appropriate to describe the cumulative characteristic of soil particles, which reflects the particle size distribution and the randomness of pore networks, thereby primarily governing physicomechanical properties, including porosity and permeability coefficient.

3.3. Mass Fractal Dimension Evaluation on the Seepage Erosion Process. As described previously, the mass fractal dimension can be used to give a good description of mass cumulative characteristics, but it is difficult to directly demonstrate the penetrating performance of porous soil. Once seepage erosion occurs, such as piping, fine particles are continuously moving from the seepage channel, resulting in a reduction in cumulative mass, rendering the varying mass fractal dimension. Both the permeability coefficient and the porosity are changed accordingly. Specifically, finer particles move via the voids of the coarser fraction under the condition of a certain hydraulic gradient, resulting in the increasing porosity of the soil. As the seepage velocity continues to increase, the fine particles begin to be removed by the seepage flow, which again increases the porosity. Subsequently, the seepage velocity is continuously increasing to wash out the larger particles from the gradually expanded leakage passage, which leads to the loss of cumulative mass in the seepage erosion process. Inversely, the changing trend of the mass fractal dimension can be used to evaluate the seepage erosion. Therefore, the objectives of this section are as follows: (i) to understand the entire process of the seepage erosion by the observations of experimental data, (ii) to analyze the mass fractal dimension between the permeability coefficient and porosity in the seepage erosion, and (iii) to show the varying trend of the mass fractal dimension in porous soil before and after the seepage erosion.

As observed in the hydraulic tests, the entire process of seepage erosion can be qualitatively divided into four phases: incubation, formation, evolution, and destruction (Figure 9). Experimental results show that there is a difference between hydraulic and mechanical characteristics in every phase of the seepage erosion process. First, in the incubation phase, soil particles are almost static, and soil skeletons are stable without any soil deformation under a low hydraulic gradient. Next, in the formation phase, the surface grains are slowly adjusted, resulting in progressive soil deformation, while soil skeletons are still stable with the increasing hydraulic gradient. At this point, the viscous shear force and the seepage force on the soil grains reach the magnitude of the retaining forces at exit. However, the migration of soil particles enlarges the size of the surrounding interstitial voids. As a result, the slight deformation appears and then gradually expands to nearly two-thirds of the seepage path length and eventually induces the whole deformation. Both sandy gravels and coarse-grained sand skeletons are still stable, and their deformations are not apparent in this phase. Then, in the evolution phase, the surface grains move rapidly until the void ratio reaches the maximum as the hydraulic gradient across the sample is again increased. An additional increase in the gradient reduces the downward force of the upper grains on the next layer of underlying grains, allowing them to loosen when reaching a state of equilibrium. At this point, soil skeletons are movable, and the leakage pathway is gradually expanded with the uplifting fine particles. This evolution process is continuous as the increasing gradient across the sample unless the loosened zone develops quickly in the exit face of the sample

Table 2: The mass fractal dimensions and scale-invariant intervals in different experimental soils.

Soil number	Soil type	Scale-invariant interval		Fine content of scale-invariant interval (%)	Mass fractal dimension	Correlation coefficient
		Lower limit (mm)	Upper limit (mm)			
1	Sandy gravel	0.25	20	91.75	2.84	0.94
2	Sandy gravel	0.25	20	88.83	2.65	0.95
3	Sandy gravel	0.25	20	87.70	2.61	0.99
4	Sandy gravel	0.25	20	87.17	2.57	0.98
5	Coarse-grained sand	0.25	10	68.98	2.87	0.99
6	Coarse-grained sand	0.25	10	68.54	2.84	0.94
7	Fine-grained sand	0.25	5	57.42	2.90	0.79
8	Fine-grained sand	0.25	5	65.49	2.99	0.91

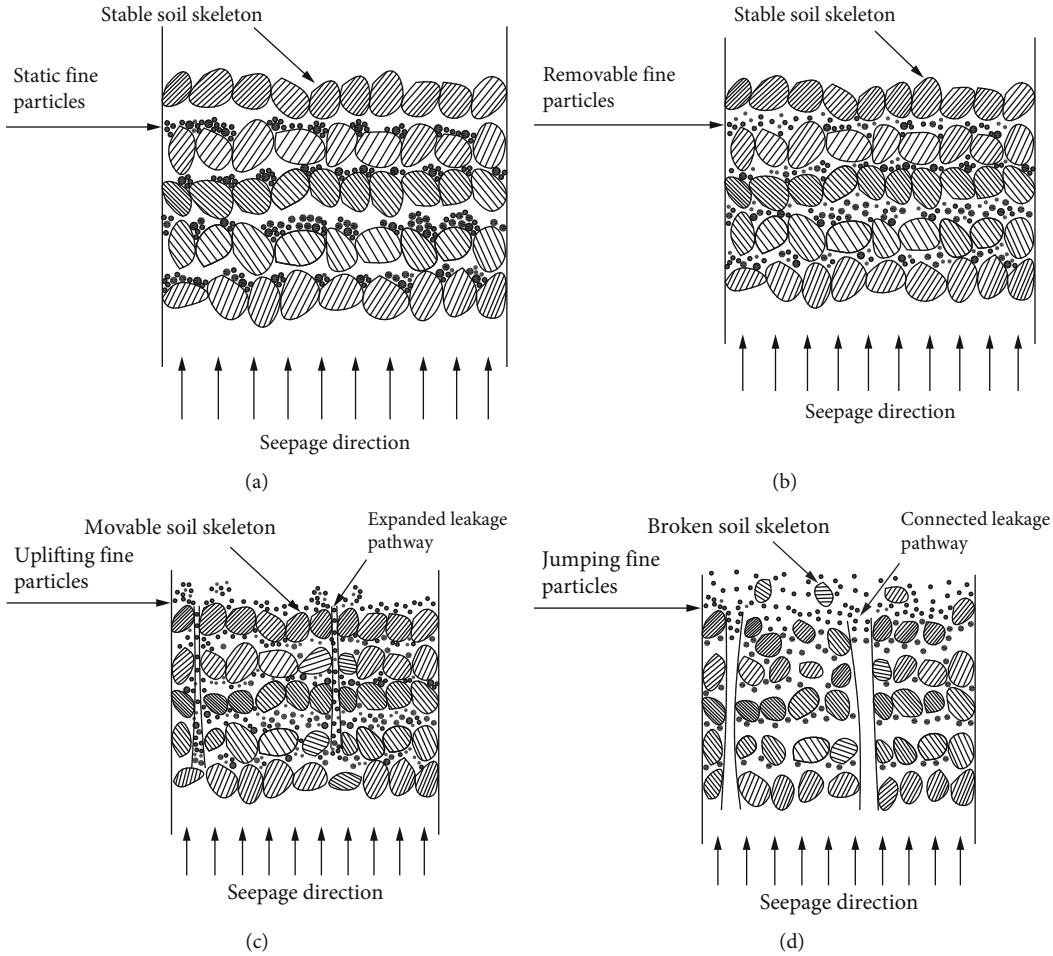

Figure 9: Schematic illustration of the entire seepage erosion process observed in the hydraulic tests: (a) incubation, (b) formation, (c) evolution, and (d) destruction.

progressively heaves. Last, in the destruction phase, sand boil or total heave appears when a random alignment of the large interstitial void is formed in the near-surface soil structure, thus producing a preferential low resistance pathway of seepage flow. The connected leakage pathway, namely, the seepage channel, acts similar to a relief well, allowing water to escape from the soil sample. The preferential pathway pressure from increased gradients is relieved without further progression of the heave due to the constant overflow of water. The removal of the fine

grains increases the permeability coefficient of the soil surrounding the preferential pathway, which expands the pathway in offering drainage to the interior of the sample. Since the seepage force continues to act on the upper grains, the process of progressively achieving equilibrium may not be maintained. Finally, the leakage pathway connects from the upstream side to the downstream side of the soil sample, accompanied by observations of jumping fine particles in groups and broken soil skeletons.

The relation between the mass fractal dimension and the porosity is shown in the seepage erosion process (Figure 10). The experimental values of porosity show an increasing trend with a little fluctuation with the development of seepage erosion, which agrees well with the experimental results of Chen et al. [31]. The maximum relative error is less than 10%, probably caused by the basic assumptions of formula deduction and the systematic errors of test measurement. At different phases of the seepage erosion process, the mass fractal dimension decreases as the porosity increases, apparently in the evolution and destruction phases, while not obviously in the phases of incubation and formation. It can be explained that fine particles transport constantly from the gradually expanded leakage pathway or pore channel (Figures 9(c) and 9(d)) at the critical hydraulic gradient, resulting in increasing porosity and decreasing fractal dimension. By comparison, since fine particles begin to move slowly at a small hydraulic gradient (Figures 9(a) and 9(b)), the leakage pathway has not been completely formed in the incubation and formation phases, thus slightly influencing the mass fractal dimension and the porosity.

The relation between the mass fractal dimension and the permeability coefficient is shown in the seepage erosion process (Figure 11). The experimental values of the permeability coefficient show an increasing trend with the development of seepage erosion, which is basically consistent with the experimental results of Zhu et al. [32]. The maximum relative error is only 8%, which is associated with the sample difference and experimental conditions. At different phases of the seepage erosion process, the mass fractal dimension decreases with the increasing permeability coefficient, which is slight in the incubation and formation phases and significant in the evolution and destruction phases. Note that the seepage force acting on the soil particles needs to overcome the viscous resistance derived from film water at an initial hydraulic gradient in the incubation and formation phases. As the hydraulic gradient increases, fine particles are continuously washed out from the leakage pathway in the phases of evolution and destruction (Figures 9(c) and 9(d)). Subsequently, the cumulative soil particles are lessened and the percolating capacity is improved at a large hydraulic gradient. As a result, the mass fractal dimension decreases while the permeability coefficient increases, which is similar to the varying law between the mass fractal dimension and the porosity mentioned above.

The mass fractal dimension changes in different soil samples are shown before and after seepage erosion (Figure 12). The mass fractal dimension before seepage erosion may derive from the original grading curves, while

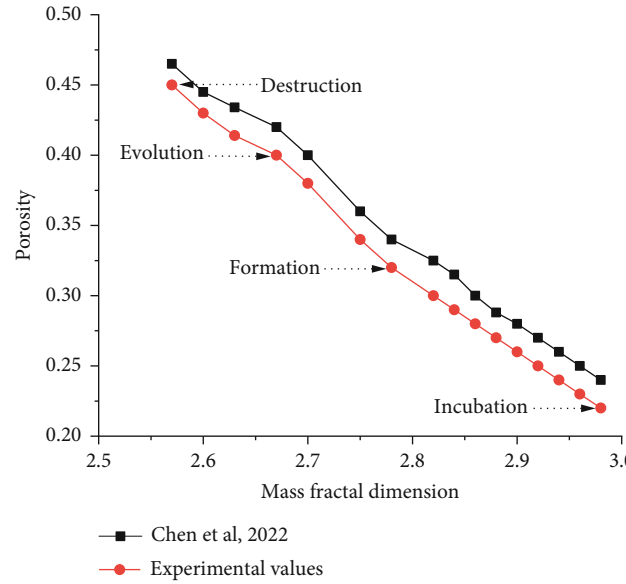

Figure 10: Relation between mass fractal dimension and porosity in the seepage erosion process.

the mass dimension after seepage erosion can be obtained from the redistributed grading curves due to the sand washed out by overflow water. According to the turbidity of the overflow water and the amount of the gushing sand, the mass fractal dimensions of all the soil samples tend to decrease to different degrees after the seepage erosion. For sandy gravel samples, a large amount of turbid water overflows, carrying the sands away at the critical hydraulic gradient. By sieving and measuring the gushing sands, it is discovered that the washout sand size was less than 0.50 mm, and the percentages of those sands (1#~4#) were 18%, 15%, 13%, and 17%, respectively. Correspondingly, the ratios of the mass fractal dimension fell by 6.7%, 5.0%, 4.8%, and 6.5%. For coarse sand samples, the overflow water is little turbid, accompanied by the gushing sand size of less than 0.25 mm, and the percentages of these sands (5#~6#) were 9% and 8%, respectively. The ratios of the mass fractal dimension were accordingly reduced by 4.2% and 4.1%. Comparatively, the overflow water through the fine sand samples was slightly turbid, with the observation of less than 0.10 mm of gushing sand at the large hydraulic gradient. It was found that the percentages of the gushing sands (7#~8#) were 5%and 4%, respectively, and the ratios of the mass fractal dimension dropped to 2.3%and 2.2%, respectively.

The relationship between the mass fractal dimension, permeability coefficient, and porosity can provide a reference for the choice of physicomechanical parameters of porous soil in engineering practice. Based on the soil composition reported in geotechnical investigation, grading curves can be drawn and then transformed with double logarithmic coordinates. The scale-invariant interval is determined, and the mass fractal dimension can be figured out. Through the above discussion, it is verified that the mass fractal dimension represents the accumulation characteristics of soil particles, integratively reflecting the

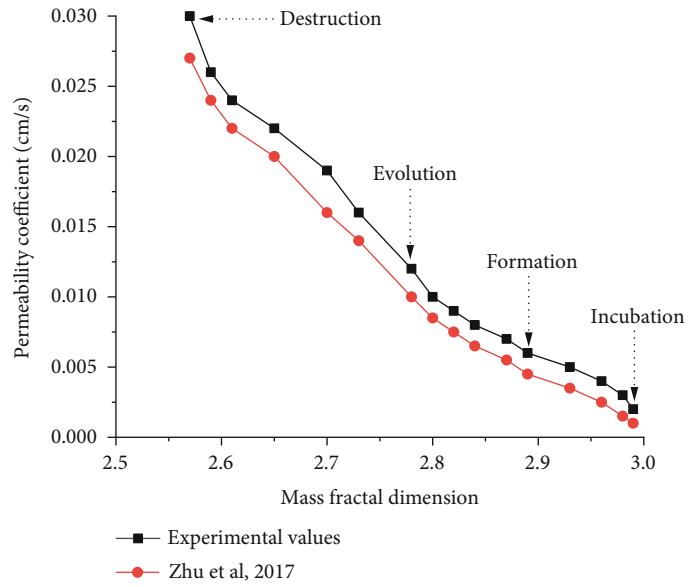

Figure 11: Relation between mass fractal dimension and permeability coefficient in the seepage erosion process.

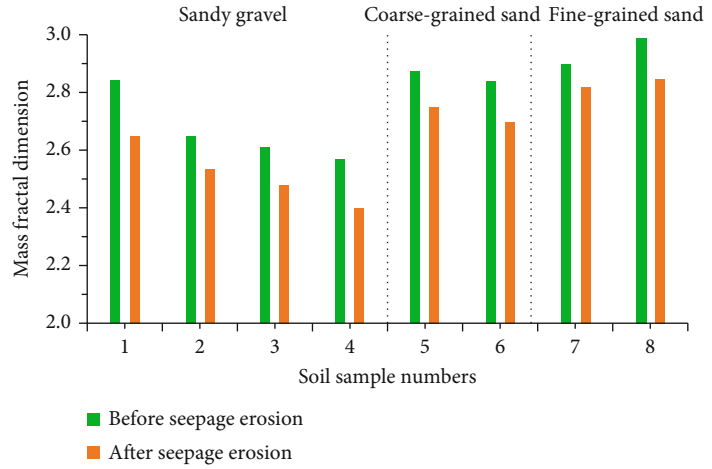

Figure 12: Mass fractal dimension changes before and after seepage erosion in soil samples.

content of fine particles, the uniformity coefficient, the porosity, and the permeability. Moreover, the changing trend of the mass fractal dimension can be used to predict the development of seepage erosion, which provides a novel approach to investigate the potential risk of seepage erosion in porous soil.

4. Summary and Conclusions

In this study, a series of hydraulic tests were carried out to show the seepage erosion process. The mass fractal dimension is used to determine the scale-invariant intervals of porous soil and to evaluate the fractal characteristics of the seepage erosion process in porous soil. The main conclusions are as follows:

(1) The mass fractal dimension is an intrinsic parameter to describe the complicated composition of porous soil, which is appropriate to describe the cumulative mass distribution of particles, the complexity of pore networks, and the dynamic changes of the seepage erosion process. Hydraulic tests have proven that the mass fractal dimension is closely related to the fine content, the porosity, and the permeability coefficient, thus largely determining the physicomechanical properties of porous soil

(2) The determination of the scale-invariant interval is an essential precondition for the accurate calculation of the mass fractal dimension. Both the average grain size and the fine content of the scale-invariant interval are the primary factors influencing the mass fractal dimension. In addition, the scale-invariant interval of sandy gravel ranges from 0.25 mm to 20 mm, while coarse-grained sand ranges from 0.25 mm to 10 mm and fine-grained sand ranges from 0.25 mm to 5 mm

(3) The seepage erosion process can be qualitatively divided into incubation, formation, evolution, and destruction. The changing law of porosity and permeability coefficient with the fractal dimension is approximately similar in the seepage erosion process. Both porosity and permeability coefficients show an increasing trend with the development of seepage erosion. However, the fractal dimension decreases due to the removal of fine particles induced by seepage flow water

The methods and results may be of interest to industrial geologists, hydrologists, and engineers who focus on seepage erosion in porous soil and theory researchers who seek to validate the applicability of fractal models. This paper is limited by hydraulic tests to sandy gravels, coarse-grained sands, and fine-grained sands. Further research with a wider variety of porous soil types and more advanced visualization technology is needed to provide more insights into the mechanisms of the seepage erosion process.

Symbols

A: Cross-sectional area (L^2)
C: Constant (-)
C_u: Uniformity coefficient (-)
D_f: Pore fractal dimension (-)
D_m: Mass fractal dimension (-)
D_T: Tortuosity fractal dimension (-)
d_{50}: Average grain size (L)
e: Void ratio (-)
i: Hydraulic gradient (-)
K: Permeability coefficient (LT^{-1})
K_0: Pore shape factor (-)
K_s: Slope (-)
L: Measure length (L)
M_T: Total mass (M)
n: Porosity (-)
R: Correlation coefficient (-)
r: Sieve size opening (L)
r_L: Maximum particle size (L)
s_0: Specific surface area (L^2)
T: Pore tortuosity (-)
γ: Fluid unit weight (MT^{-3})
μ: Fluid viscosity (MLT^{-1})
ρ_d: Dry density (MT^{-3})
λ_{max}: Maximum pore size (L).

Data Availability

The data used to support the findings of this study are available from the corresponding author upon request.

Conflicts of Interest

The authors declare that there is no conflict of interests regarding the publication of this article.

Acknowledgments

This work was supported by the University Natural Science Foundation of Jiangsu Province (Grant No. 21KJB560015), the National Natural Science Foundation of China (Grant No. 51979175), and the Fundamental Research Foundation of the Central Public Welfare Research Institutes (Grant No. Y119008).

References

[1] W. Ye, F. H. Ma, J. Hu, and Z. Y. Li, "Seepage behavior of an inclined wall earth dam underfluctuating drought and flood conditions," *Geofluids*, vol. 2018, Article ID 4734138, 11 pages, 2018.

[2] J. Bi, H. Zhang, X. Luo, H. Shen, and Z. Li, "Modeling of internal erosion using particle size as an extra dimension," *Computers and Geotechnics*, vol. 133, no. 6, p. 104021, 2021.

[3] N. Bird, M. C. Díaz, A. Saa, and A. M. Tarquis, "Fractal and multifractal analysis of pore-scale images of soil," *Journal of Hydrology*, vol. 322, no. 1-4, pp. 211–219, 2006.

[4] P. C. Carman, *Flow of Gases through Porous Media*, Academic Press, New York, 1956.

[5] X. Chao, W. Tian, F. Xu, and D. Shou, "A fractal model of effective mechanical properties of porous composites," *Composites Science and Technology*, vol. 213, no. 8, p. 108957, 2021.

[6] R. P. Chapuis, "Predicting the saturated hydraulic conductivity of soils: a review," *Bulletin of Engineering Geology and the Environment*, vol. 71, no. 3, pp. 401–434, 2012.

[7] J. P. De Bono and G. R. McDowell, "On the packing and crushing of granular materials," *International Journal of Solids and Structures*, vol. 187, no. 7, pp. 133–140, 2020.

[8] M. Glenn and D. B. John, "Relating hydraulic conductivity to particle size using DEM," *International Journal of Geomechanics*, vol. 21, no. 1, p. 06020034, 2021.

[9] D. M. Gu, D. Huang, H. L. Liu, W. G. Zhang, and X. C. Gao, "A DEM-based approach for modeling the evolution process of seepage-induced erosion in clayey sand," *Acta Geotechnica*, vol. 14, no. 6, pp. 1629–1641, 2019.

[10] I. Kobayshi, H. Owada, T. Ishii, and A. Lizuka, "Evaluation of specific surface area of bentonite-engineered barriers for Kozeny-Carman law," *Soils and Foundations*, vol. 57, no. 5, pp. 683–697, 2017.

[11] B. Li, R. Liu, and Y. Jiang, "A multiple fractal model for estimating permeability of dual-porosity media," *Journal of Hydrology*, vol. 540, no. 9, pp. 659–669, 2016.

[12] B. B. Mandelbrot, *The Fractal Geometry of Nature*, W. H. Freemanand Company, New York, 1982.

[13] S. Qiu, M. Yang, P. Xu, and B. Rao, "A new fractal model for porous media based on low-field nuclear magnetic resonance," *Journal of Hydrology*, vol. 586, no. 3, p. 124890, 2020.

[14] X. Ren, Y. Zhao, Q. Deng, and D. Wang, "A relation of hydraulic conductivity — void ratio for soils based on Kozeny-Carman equation," *Engineering Geology*, vol. 213, no. 12, pp. 89–97, 2016.

[15] K. S. Richards and K. R. Reddy, "Experimental investigation of initiation of backward erosion piping in soils," *Geotechnique*, vol. 62, no. 10, pp. 933–942, 2012.

[16] J. S. Shepard, "Using a fractal model to compute the hydraulic conductivity function," *Soil Science Society of America Journal*, vol. 57, no. 2, pp. 300–306, 1993.

[17] K. L. Tian, A. Q. Yang, K. Y. Nie, H. L. Zhang, J. Xu, and X. D. Wang, "Experimental study of steady seepage in unsaturated loess soil," *Acta Geotechnica*, vol. 15, no. 9, pp. 2681–2689, 2020.

[18] D. L. Turcotte, *Fractals and Chaos in Geology and Geophysics*, Cambridge University Press, New York, 2012.

[19] S. W. Tyler and S. W. Wheateraft, "Fractal scaling of soil particle-size distributions: analysis and limitations," *Soil Science Society of America Journal*, vol. 56, no. 2, pp. 362–369, 1992.

[20] Y. Wang, S. J. Wang, X. B. Duan, Y. C. Gu, Q. Pang, and C. Yang, "Physical modelling of initial seepage failure process," *International Journal of Physical Modelling in Geotechnics*, vol. 15, no. 4, pp. 1–9, 2015.

[21] S. W. Wheatcraft and S. W. Tyler, "An explanation of scale-dependent dispersivity in heterogeneous aquifers using concepts of fractal geometry," *Water Resources Research*, vol. 24, no. 4, pp. 566–578, 1988.

[22] A. Wörman and R. Olafsdottir, "Erosion in a granular medium interface," *Journal of Hydraulic Research*, vol. 30, no. 5, pp. 639–655, 1992.

[23] M. Wu, J. Liu, X. Lv, D. Shi, and Z. Zhu, "A study on homogenization equations of fractal porous media," *Journal of Geophysics and Engineering*, vol. 15, no. 6, pp. 2388–2398, 2018.

[24] Y. Xia, J. Cai, E. Perfect, W. Wei, Q. Zhang, and Q. Meng, "Fractal dimension, lacunarity and succolarity analyses on CT images of reservoir rocks for permeability prediction," *Journal of Hydrology*, vol. 579, no. 2, article 124198, 2019.

[25] W. Xu, M. Jia, and Z. Gong, "Thermal conductivity and tortuosity of porous composites considering percolation of porous network: from spherical to polyhedral pores," *Composites Science and Technology*, vol. 167, no. 7, pp. 134–140, 2018.

[26] B. M. Yu and P. Cheng, "A fractal permeability model for bi-dispersed porous media," *International Journal of Heat and Mass Transfer*, vol. 45, no. 14, pp. 2983–2993, 2002.

[27] B. M. Yu, "Analysis of flow in fractal porous media," *Applied Mechanics Reviews*, vol. 61, no. 5, article 050801, 2008.

[28] B. M. Yu, J. H. Li, Z. H. Li, and M. Q. Zou, "Permeabilities of unsaturated fractal porous media," *International Journal of Multiphase Flow*, vol. 29, no. 10, pp. 1625–1642, 2003.

[29] B. M. Yu and J. H. Li, "Some fractal characters of porous media," *Fractals*, vol. 9, no. 3, pp. 365–372, 2001.

[30] X. D. Ni, Y. L. Niu, Y. Wang, and K. Yu, "Non-Darcy flow experiments of water seepage throughrough-walled rock fractures," *Geofluids*, vol. 2018, Article ID 8541421, 12 pages, 2018.

[31] B. Chen, J. Deng, M. J. Hu, J. L. Zhang, and T. Zhang, "Macro and micro experimental study on fractal fragmentation characteristics of calcareous sand during one-dimensional creep," *Chinese Journal of Rock and Soil Mechanics*, vol. 43, no. 7, pp. 1–11, 2022.

[32] S. Zhu, S. D. Deng, Z. Y. Ning, and J. Wang, "Gradation design method for rockfill materials based on fractal theory," *Chinese Journal of Geotechnical Engineering*, vol. 39, no. 6, pp. 1151–1155, 2017.

[33] D. Ma, H. Y. Duan, J. X. Zhang, X. J. Feng, and Y. L. Huang, "Experimental investigation of creep-erosion coupling mechanical properties of water inrush hazards in fault fracture rock masses," *Chinese Journal of Rock Mechanics and Engineering*, vol. 40, no. 9, pp. 1751–1763, 2021.

[34] D. Ma, W. T. Hou, J. X. Zhang, J. J. Wang, Z. H. Li, and D. Feng, "Radial seepage-axial stress characteristics of hollow rock sample andseepage mutation mechanism of roadway surrounding rock," *Journal of China Coal Society*, vol. 21, pp. 1–18, 2022.

[35] D. Ma, H. Y. Duan, X. B. Li, Z. H. Li, Z. Zhou, and T. B. Li, "Effects of seepage-induced erosion on nonlinear hydraulic properties of broken red sandstones," *Tunnelling and Underground Space Technology*, vol. 91, no. 9, p. 102993, 2019.

[36] D. Ma, H. Y. Duan, W. T. Liu, X. T. Ma, and M. Tao, "Water–sediment two-phase flow inrush hazard in rock fractures of overburden strata during coal mining," *Mine Water and the Environment*, vol. 39, no. 2, pp. 308–319, 2020.

[37] J. F. Bi, H. T. Zhang, X. Q. Luo, H. Shen, and Z. M. Li, "Size distribution of free particles in soils: a geometric modelling approach," *Acta Geotechnica*, vol. 16, no. 12, pp. 3849–3866, 2021.

[38] H. B. Zhao, H. Zhang, H. H. Li, F. H. Wang, and M. Zhang, "Formation and fractal characteristics of main fracture surface of red sandstone under restrictive shear creep," *International Journal of Rock Mechanics and Mining Sciences*, vol. 98, pp. 181–190, 2017.

[39] S. Zendehboudi, N. Rezaei, and A. Lohi, "Applications of hybrid models in chemical, petroleum, and energy systems: a systematic review," *Applied Energy*, vol. 228, pp. 2539–2566, 2018.

[40] T. Yan, W. Li, and X. L. Bi, "Research on effective stress model in porous media based on fractal method," *Chinese Journal of Rock and Soil Mechanics*, vol. 31, no. 8, pp. 2625–2629, 2010.

[41] S. M. He, X. X. Zhang, and Y. Wu, "Study of stability discriminant of slope and position determination of potentialsliding surface based on upper bound theorem," *Chinese Journal of Rock and Soil Mechanics*, vol. 33, no. 1, pp. 162–166, 2012.

[42] M. Seyyedattar, S. Zendehboudi, and S. Butt, "A comprehensive review on fluid and rock characterization of offshore petroleum reservoirs: tests, empirical and theoretical tools," *Journal of Porous Media*, vol. 22, no. 13, pp. 1697–1755, 2019.

[43] M. Sheng, G. Li, S. Tian, Z. W. Huang, and L. Q. Chen, "A fractal permeability model for shale matrix with multi-scale porous structure," *Fractals*, vol. 24, no. 1, pp. 1650002–1650011, 2016.

[44] A. Behrang, P. Mohammadmoradi, S. Taheri, and A. Kantzas, "A theoretical study on the permeability of tight media; effects of slippage and condensation," *Fuel*, vol. 181, pp. 610–617, 2016.

[45] W. H. Song, D. Y. Wang, J. Yao et al., "Multiscale image-based fractal characteristic of shale pore structure with implication to accurate prediction of gas permeability," *Fuel*, vol. 241, pp. 522–532, 2019.